

*Journal of*  
***Mechanics of***  
***Materials and Structures***

**THE SHEAR RESPONSE OF METALLIC SQUARE HONEYCOMBS**

François Cote, Vikram S. Deshpande and Norman A. Fleck

*Volume 1, N° 7*

*September 2006*



mathematical sciences publishers

## THE SHEAR RESPONSE OF METALLIC SQUARE HONEYCOMBS

FRANÇOIS COTE, VIKRAM S. DESHPANDE AND NORMAN A. FLECK

Stainless steel square honeycombs have been manufactured by slotting together steel sheets and then brazing the assembly. Their out-of-plane shear response is measured as a function of the relative density of the honeycomb and of the direction of shearing with respect to the material axes of the square honeycomb. The response is nearly isotropic with the shear strength and reasonably insensitive to the loading direction. In contrast to the out-of-plane compressive response, the shear response is monotonically hardening and the shear strength scales linearly with relative density. A simple analytical model based upon uniform deformation of the cell walls is in good agreement with the measured shear behavior at low shear strains, and predicts the onset of wrinkling of the cell walls to reasonable accuracy. Finite element (FE) calculations are accurate up to large values of shear strain, and reveal that the shear strength of the square honeycombs is relatively insensitive to the ratio of honeycomb height to cell size. The shear strength of square honeycombs compares favorably with other competing sandwich core topologies such as pyramidal and corrugated truss cores.

### 1. Introduction

The development of metallic micro-architected materials for application as the cores of sandwich structures is of current academic and industrial interest. Three classes of core architecture have been proposed: prismatic cores, 3D trusses, and honeycombs. The most suitable choice of sandwich core architecture depends upon the specific application. For example, trusses with their open celled architecture are ideal for multifunctional applications involving heat transfer in addition to load carrying capacity [Evans et al. 2001]. On the other hand, these sandwich cores have a low in-plane stretching strength. Thus, for load-bearing, honeycomb cores are superior to the truss cores. Traditionally, hexagonal honeycombs have been extensively employed in sandwich construction [Gibson and Ashby 1997]. Similar to the truss cores, these hexagonal honeycombs suffer from the drawback of low in-plane stretching strength. Square honeycombs overcome this drawback, at least for loadings along the directions of the cell walls, and thereby have promise for sandwich construction. The out-of-plane shear properties of stainless steel square honeycombs are the focus of this study. The out-of-plane loading direction is of particular importance in sandwich beams and plates since the core functions by carrying shear loads while the face sheets carry bending loads.

---

The authors are grateful to ONR for their financial support through US-ONR IFO grant number N00014-03-1-0283 on The Science and Design of Blast Resistant Sandwich Structures. FC acknowledges support from the Cambridge Commonwealth Trust and the Fonds Québécois de la Recherche sur la Nature et les Technologies.

*Keywords:* honeycombs, wrinkling, shear strength, sandwich panels.

Honeycombs usually comprise hexagonal cells and are manufactured by either an expansion or corrugation process. For example, see the Hexcel Composites<sup>1</sup> honeycomb data sheet [Hexcel 1999]. Hexagonal honeycombs are routinely employed as the cores for lightweight sandwich panels and as energy absorbers. They are typically manufactured from aluminum (Al) alloys and have a relative density  $\bar{\rho}$  (that is, the ratio of the density of the honeycomb treated as a homogeneous continuum to the density of the solid) of less than 3%. Experiments and simple analyses have shown that their out-of-plane elastic properties scale linearly with the relative density  $\bar{\rho}$  [Kelsey et al. 1958; Zhang and Ashby 1992]. In out-of-plane crushing, these honeycombs exhibit a stress peak followed by large stress oscillations associated with the formation of a succession of plastic folds in each cell. Similarly the out-of-plane peak shear strength is governed by cell wall buckling [Werren and Norris 1950; Zhang and Ashby 1992]. Once the wrinkles have formed, the shear stress drops and subsequently remains approximately constant until failure occurs by the fracture of the cell walls. Experimental studies illustrating this behavior have been presented by [Doyoyo and Mohr 2003; Mohr and Doyoyo 2004b] and the corresponding numerical simulations of the shear response of Al hexagonal honeycombs by [Mohr and Doyoyo 2004a]. Most experimental studies are restricted to relative densities  $\bar{\rho} < 0.08$ , since debonding of the honeycombs from the plates of the single-lap shear fixture has been observed for both metallic [Hexcel 1999] and nonmetallic honeycombs [Werren and Norris 1950; Zhang and Ashby 1992] at higher relative densities.

Recent studies [Fleck and Deshpande 2004; Xue and Hutchinson 2004] suggest that square honeycomb cores having a high relative density ( $\bar{\rho} > 0.05$ ) are preferable for high-severity loadings such as blasts and shocks because of their high out-of-plane crushing resistance and high in-plane stretching strength. We expect enhanced performance of square honeycombs constructed from solids of high strain hardening, such as stainless steels. An experimental investigation into the out-of-plane compressive response of stainless square honeycombs by [Côté et al. 2004] over a relative density range  $0.03 < \bar{\rho} < 0.2$  confirmed that the honeycombs exploit the strain hardening behavior of the stainless steel. Peak compressive strength is set by the axial torsional plastic buckling of the square honeycomb cells. In fact, no progressive folding of the cell walls was observed by [Côté et al. 2004]. This difference in compressive response between aluminum and stainless steel honeycombs is attributed to differences in the strain hardening response of the parent materials.

The objectives of the present study are to investigate the effects of the relative density  $\bar{\rho}$ , shear loading direction, and cell aspect ratio (that is, the ratio of cell height-to-cell size) on the out-of-plane shear response of stainless steel square honeycombs. First, we describe the procedure used to manufacture stainless steel square honeycomb and our test protocol. Second, we report the observed the out-of-plane shear behavior, including the effects of relative density and loading direction. We compare these experimental measurements with a simple analytical model and 3D finite element simulations. Finally, we compare the shear response of the square honeycombs with that for commercially available aluminum hexagonal honeycombs, as well as three other alternative core topologies.

## 2. Experimental method

**2.1. Specimen manufacture and test protocol.** Since metallic square-honeycombs are not yet commercially manufactured, we manufactured them by electro-discharge machining and brazing as described

---

<sup>1</sup>Hexcel Composites, Duxford, Cambridge, CB2 4QD, United Kingdom.

below. Square honeycombs were manufactured from AISI type 304 stainless steel sheets of thickness  $t = 0.30$  mm, using the slotting technique of [Côté et al. 2004; Côté et al. 2006]. The sheets were cropped into long strips of height  $H$ . Cross-slots of width  $0.305$  mm and spacing  $l$  in the range  $6$  to  $17.5$  mm were cut by electro-discharge machining (EDM). To first order in  $t/l$ , the relative density  $\bar{\rho}$  of the square honeycomb is  $\bar{\rho} = 2t/l$ . Four relative densities of square honeycomb specimens were manufactured and tested by varying the cell size  $l$ .

The square honeycombs were assembled by slotting together the sheets as shown in Figure 1a. A clearance of  $5 \mu\text{m}$  between sheet and slot facilitated assembly while providing a sufficiently tight fit to

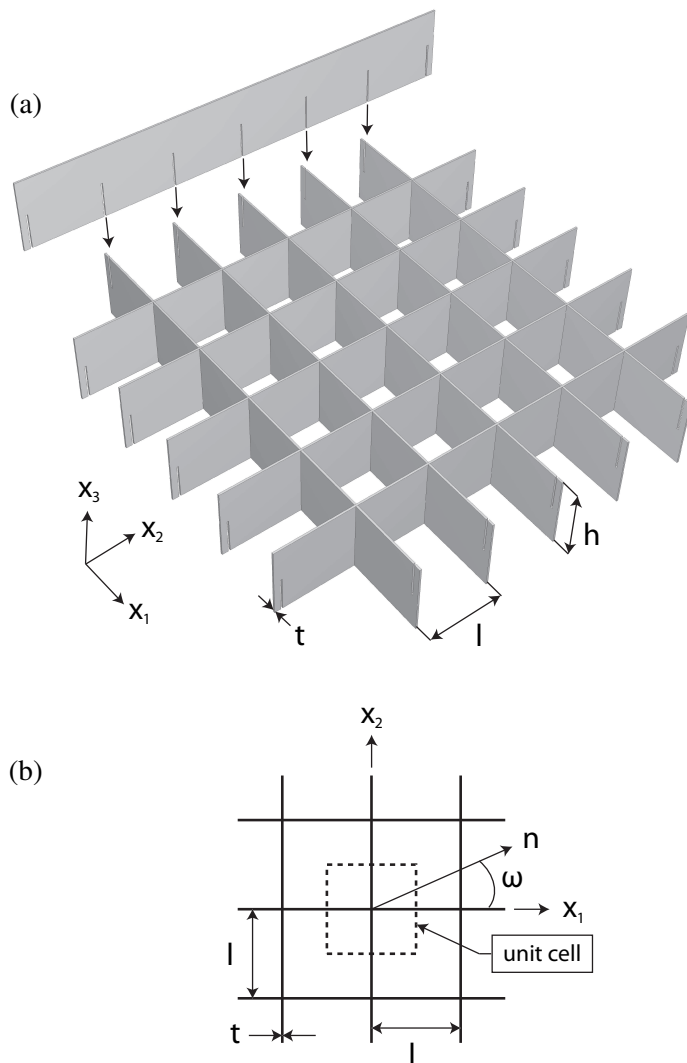


**Figure 1.** (a) Sketch of the square honeycomb manufacturing technique. (b) Schematic of the unit cell employed in the finite element analysis, including the coordinate system adopted and the loading direction  $n$ .

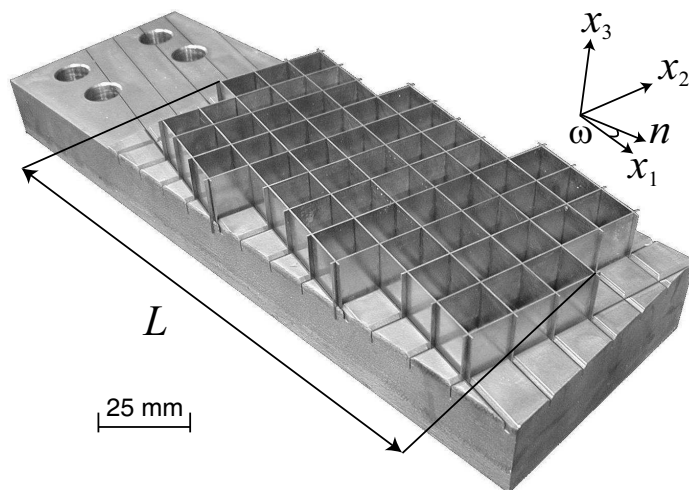


**Figure 2.** Photograph of  $a\bar{\rho} = 0.05$  square honeycomb specimen slotted into one of the faces of the single-lap shear test fixture. This specimen is loaded in the  $\omega = \tan^{-1}(1/4)$  direction.

assure stability. To ensure good bonding between the square honeycomb specimens and the shear test fixture, slots of width 0.31 mm and depth 4 mm were electro-discharge machined into 25 mm thick steel sheets. These steel sheets served as the test fixtures. The cross-slotted square honeycomb specimens were then assembled onto the test fixtures as shown in Figure 2. Consequently, the net height of the honeycomb was  $h = H - 8$  mm.

After assembly of the honeycomb core into the single-lap shear test fixture, the braze alloy Ni-Cr 25-P10 (wt.%) was applied uniformly over the sheets of the square honeycombs and the inner surfaces of the test fixture. The whole assembly was then brazed together in a vacuum furnace at 1075° C in a dry argon atmosphere at 3–10 Pa. Capillarity forces were sufficient to draw the braze into the joints, resulting in an excellent bond. After brazing, the wall thickness was measured to be  $t = 0.32$  mm. In all tests performed in this study the cell aspect ratio of the square honeycomb specimens was  $h/l = 1$ .

The quality of the braze joints was assessed by optical microscopy and SEM/EDX dot mapping techniques. The surface of a typical square-honeycomb joint was prepared by successive grinding steps and a final polish with 1  $\mu\text{m}$  diamond paste. The polished surface was then etched using a solution comprising 74% hydrochloric acid and 1.3% hydrogen peroxide. An optical photograph of a polished and etched brazed joint is shown in Figure 3 and confirms the good overall bonding at the joints. A closer inspection however reveals the presence of two phases in the joint. The composition of those phases was obtained by EDX dot mapping analysis. The first phase has approximately the composition of stainless steel, that is, Fe, Ni, and Cr, while the second phase contains phosphides and are expected to decrease the ductility of the joint [Zhuang and Eagar 1997].

We defined  $x_3$  as the out-of-plane direction, and  $n$  as the unit vector in the  $x_1 - x_2$  plane at an angle  $\omega$  to the  $x_1$ -direction, as sketched in Figure 1b. Then, the out-of-plane shear response  $\tau_{3n} - \gamma_{3n}$  was measured using the single-lap shear set-up, with selected values of  $\omega$ . All tests were performed in accordance

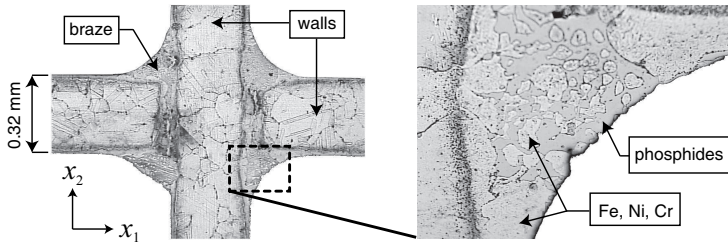


**Figure 3.** Photograph of a polished braze joint showing the effect of diffusion bonding on the microstructure of the joint. The zoom area reveals the presence of two phases in the joint.

with [ASTM 2000] for shear tests on sandwich cores. The standard demands a specimen aspect ratio of  $L/h \geq 12$ , where  $L$  is the length of the specimen. The example shown in Figure 2 is for a  $\bar{\rho} = 0.05$  square honeycomb specimen, loaded in the  $\omega = \tan^{-1}(1/4)$  direction.

The shear tests were performed on a 150 kN screw driven test machine at an applied macroscopic nominal shear strain-rate of  $10^{-4} \text{ s}^{-1}$ . The load was measured by the load cell of the test machine and was used to define the nominal shear stress. A clip gauge mounted on the single-lap shear test fixture was employed to measure the relative displacement between the two faces of the square honeycomb specimens, thereby giving the applied shear strain. A photograph of the overall single-lap shear test

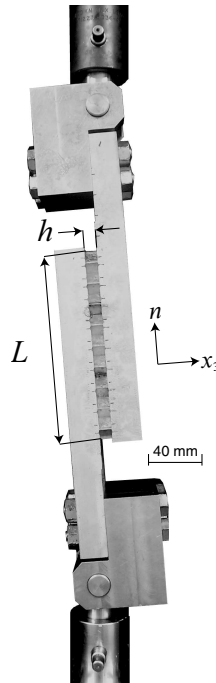


**Figure 4.** Photograph of the single-lap shear test fixture, with  $a\bar{\rho} = 0.05$  square honeycomb specimen loaded in the  $\omega = \pi/4$  direction.

fixture with a  $\bar{\rho} = 0.05$  square honeycomb specimen loaded in the  $\omega = 45^\circ$  direction is shown in Figure 4. For sake of clarity, the clip gauge is not shown on the Figure 4 but was mounted during the experiments using a standard arrangement for a single-lap shear test [Kelsey et al. 1958].

**2.2. Properties of the parent material.** Tensile specimens of dog-bone geometry were cut from the 304 stainless steel sheets and subjected to the same brazing cycle as that used to manufacture the square honeycombs. The measured true tensile stress versus logarithmic strain response, shown in Figure 5, can be approximated as elastic, linearly hardening with a Young's modulus  $E = 210$  GPa, yield strength  $\sigma_y = 210$  MPa and post-yield tangent modulus  $E_y = 2.1$  GPa.

### 3. Shear response of square honeycombs

**3.1. Measurements.** The measured transverse shear stress  $\tau_{31}$  versus shear strain  $\gamma_{31}$  ( $\omega = 0^\circ$ ) response of four selected relative densities of the square honeycomb are plotted in Figure 6. In all cases, the shear stress versus strain response displays a hardening character with no stress drop.

A montage of photographs of the  $\bar{\rho} = 0.04$  specimen at selected levels of applied shear strain  $\gamma_{31}$  is given in Figure 7. The deformation of the cell walls is essentially uniform for shear strains  $\gamma_{31} < 0.02$ . Wrinkling of the cell walls is observed at larger strains, with typically two folds in each cell wall. Visual observations on the four tests plotted in Figure 6 indicate that wrinkling commenced at  $\gamma_{31} = 0.02, 0.04, 0.8$  and  $0.11$  for  $\bar{\rho} = 0.04, 0.05, 0.08$  and  $0.11$ , respectively. The observed onset of wrinkling is marked by solid circles in Figure 6.

The effect of the loading angle  $\omega$  on the shear stress  $\tau_{3n}$  versus  $\gamma_{3n}$  response of the square honeycombs is shown in Figure 8. The shear strength increases with  $\omega$  for  $0 \leq \omega \leq \pi/4$ . Note that half of the cell walls carry nearly no load when  $\omega = 0^\circ$  while all cell walls are equally loaded when  $\omega = \pi/4$ . The increase in shear strength also occurs because wrinkling of the cell walls is delayed for loading with  $\omega > 0^\circ$ . Visual observations suggest that wrinkling of the cell wall parallel to the  $x_1$  commences at  $\gamma_{3n} = 0.04, 0.05, 0.06$

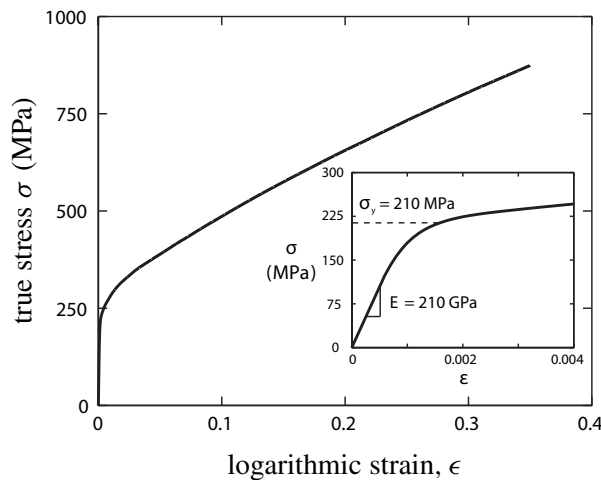


**Figure 5.** The measured tensile stress versus strain curve of the as-brazed 304 stainless steel. Tensile response was measured at an applied strain rate of  $10^{-4} \text{ s}^{-1}$ .

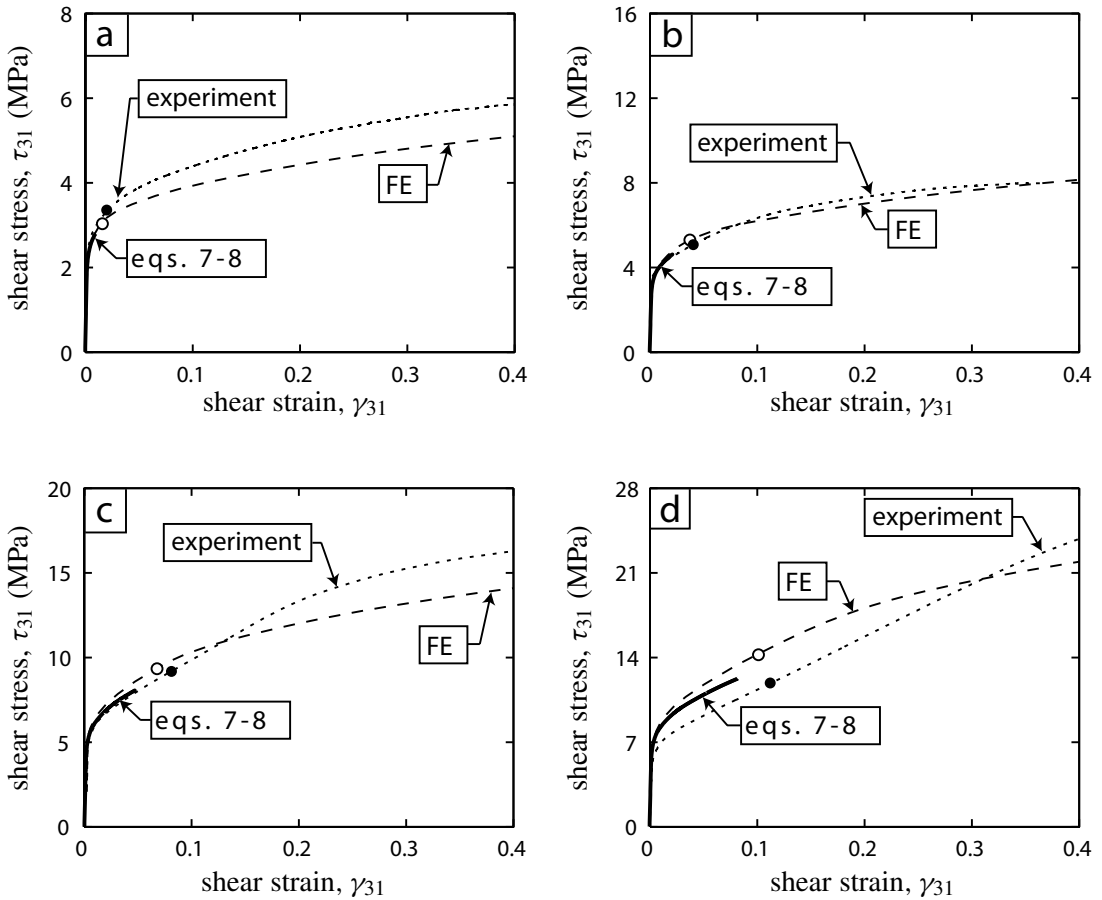


**Figure 6.** The measured response, and the FE and analytical predictions of the shear stress  $\tau_{31}$  versus shear strain  $\gamma_{31}$  response for square honeycomb specimens of differing relative density  $\bar{\rho}$  with  $\omega = 0^\circ$  of (a)  $\bar{\rho} = 0.04$ , (b)  $\bar{\rho} = 0.05$ , (c)  $\bar{\rho} = 0.08$  and (d)  $\bar{\rho} = 0.11$ . The onset of wrinkling, as observed in the experiments, and as predicted by the FE calculations, are marked as filled and open circles, respectively.

and 0.07 for loading along  $\omega = 0^\circ$ ,  $\tan^{-1}(1/4)$ ,  $\tan^{-1}(1/2)$  and  $\pi/4$ , respectively. Again, the observed onset of wrinkling is marked by the solid circles in Figure 8.

Note that the shear test fixture applies a prescribed shear strain  $\gamma_{3n}$ , and the measured shear traction is the component along the  $n$ -direction. For  $\omega \neq 0^\circ$  or  $45^\circ$  the straining direction is not aligned with symmetry axes of the honeycomb, and a finite shear traction perpendicular to the  $n$ -direction is also generated. This component of shear traction has not been measured in the current study.

**3.2. Analytical predictions.** Assuming uniform straining of the cell walls of the square honeycombs, the applied shear strain  $\gamma_{3n}$  is related to the shear strains  $\gamma_1^w$  and  $\gamma_2^w$  in the cell walls parallel to the  $x_1$  and  $x_2$  axis, respectively via

$$\gamma_1^w = \gamma_{3n} \cos \omega, \tag{1a}$$

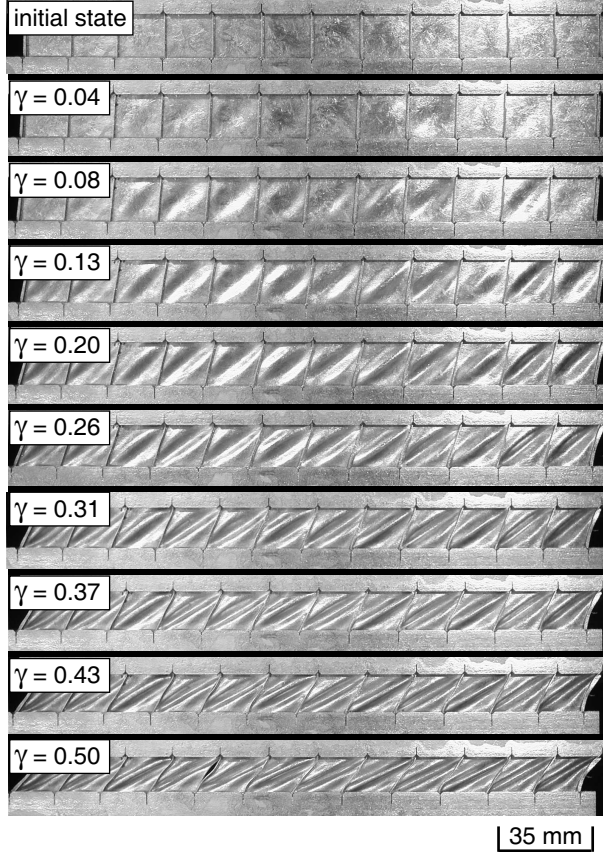


**Figure 7.** Photographs showing the deformation mode of the  $\bar{\rho} = 0.04$  square honeycomb specimen loaded in the  $\omega = 0^\circ$  direction.

$$\gamma_2^w = \gamma_{3n} \sin \omega. \tag{1b}$$

The honeycomb responds with a shear traction  $\tau_1^w$  in the cell wall parallel to the  $x_1$ -direction and with a shear traction  $\tau_2^w$  parallel to the  $x_2$ -direction. The measured shear stress  $\tau_{3n}$ , for  $0 \leq \omega \leq \pi/4$ , is

$$\tau_{3n} = (\tau_1^w \cos \omega + \tau_2^w \sin \omega) \frac{\bar{\rho}}{2}. \tag{2}$$

In general, the traction  $(\tau_2^w \cos \omega - \tau_1^w \sin \omega) \bar{\rho}/2$  transverse to the shearing direction does not vanish.

Consider first the elastic response of the honeycomb. For an applied shear strain  $\gamma_{3n}$ , the wall stresses are

$$\tau_1^w = G \gamma_{3n} \cos \omega, \tag{3a}$$

$$\tau_2^w = G \gamma_{3n} \sin \omega, \tag{3b}$$

where  $G$  is shear modulus of the cell wall material. The out-of-plane shear modulus  $G_{3n}$  of the square honeycombs is isotropic, due to its 4-fold symmetry about the  $x_3$  axis. Combining Equation (2) and

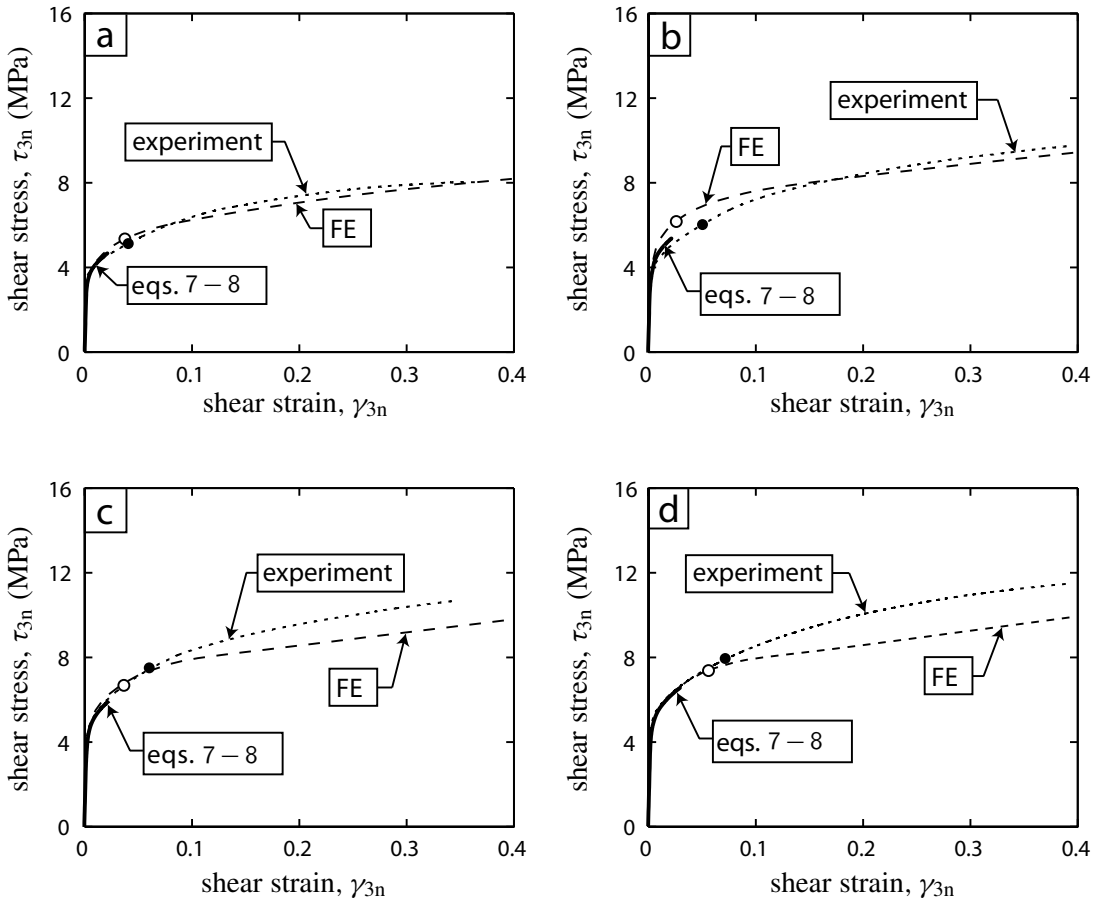


**Figure 8.** The measured response and the FE and analytical predictions of the shear stress  $\tau_{3n}$  versus shear strain  $\gamma_{3n}$  response of the  $\bar{\rho} = 0.05$  square honeycombs specimens loaded in the (a)  $\omega = 0^\circ$ , (b)  $\omega = \tan^{-1}(1/4)$ , (c)  $\omega = \tan^{-1}(1/2)$  and (d)  $\omega = \pi/4$  directions. The onset of wrinkling as observed in the experiments and predicted by the FE calculations are marked as filled and open circles, respectively.

Equations (3a) and (3b), the shear modulus  $G_{3n}$  of the square honeycombs becomes

$$G_{3n} = \frac{E}{4(1 + \nu)} \bar{\rho},$$

where  $E$  and  $\nu$  are the Young’s modulus and Poisson ratio of the isotropic solid parent material, respectively. Moreover, isotropy of elastic response dictates that the shear traction  $(\tau_2^w \cos \omega - \tau_1^w \sin \omega) \bar{\rho} / 2$  transverse to the shearing direction vanishes.

We proceed to develop an analytical model for the shear strength  $\tau_{3n}^p$  of the square honeycombs made from an elastic, ideally plastic material with a Young’s modulus  $E$ , Poisson’s ratio  $\nu$  and yield strength  $\sigma_y$ . With the cell walls modeled as thin clamped plates under shear loading, the maximum allowable shear stress of the square honeycomb is set by either elastic buckling or plastic yielding of cell walls.

The elastic shear buckling strength of a clamped plate is given by [Timoshenko and Gere 1963] as

$$\tau_c = \frac{k\pi^2 E}{12(1-\nu^2)} \left(\frac{t}{l}\right)^2, \tag{4}$$

where  $k$  varies from 8.99 to 12.28 [Timoshenko and Gere 1963], depending on the aspect ratio  $h/l$ . Note that for a honeycomb with aspect ratio  $h/l = 1$  and clamped edges along  $x_3 = 0$  and  $x_3 = h$ ,  $k = 12.28$ . For elastic behavior, Equation (3) dictates that the wall stresses are related by

$$\tau_2^w = \tau_1^w \tan \omega \tag{5}$$

and consequently, with  $\tau_1^w$  set equal to  $\tau_c$  the elastic buckling stress of the square honeycomb is

$$\tau_{3n}^p = \begin{cases} \frac{k\pi^2 E}{96 \cos \omega (1-\nu^2)} \bar{\rho}^3, & \text{if } \omega \leq 45^\circ, \\ \frac{k\pi^2 E}{96 \sin \omega (1-\nu^2)} \bar{\rho}^3, & 45^\circ < \omega \leq 90^\circ. \end{cases}$$

In contrast, when the cell walls undergo plastic deformation, Equation (5) is no longer valid. With both the cell walls assumed to be at a state of shear yield, the plastic shear strength of the square honeycomb is obtained by substituting  $\tau_2^w = \tau_1^w = \sigma_y/\sqrt{3}$  into Equation (2). (Here we assume that the tensile yield strength of the solid is related to its shear yield strength via the usual von Mises relation.) Thus, the maximum allowable shear stress of the square honeycomb made from an elastic, ideally plastic solid follows as

$$\tau_{3n}^p = \begin{cases} \frac{k\pi^2 E}{96 \cos \omega (1-\nu^2)} \bar{\rho}^3, & \text{if } \bar{\rho} < \sqrt{\frac{48(1-\nu^2)\sigma_y \cos \omega}{\sqrt{3}k\pi^2 E (\cos \omega + \sin \omega)}} \\ \frac{\sigma_y}{2\sqrt{3}} \bar{\rho} (\cos \omega + \sin \omega), & \text{otherwise,} \end{cases} \tag{6}$$

for  $0 \leq \omega \leq 45^\circ$ . The corresponding strength for loading in the  $45^\circ < \omega \leq 90^\circ$  direction follows by interchanging  $\sin \omega$  and  $\cos \omega$  in Equation (6).

Alternatively, consider parent material response for rigid strain hardening. Here we develop an analytical expression for the shear stress versus strain response of the square honeycomb prior to the development of wrinkles (that is, when the constituent sheets are in a uniform state). We assume uniform deformation of the cell walls, and write the uniaxial tensile stress versus plastic strain response of the cell wall material as  $\sigma(\varepsilon)$ . With the macroscopic shear strain  $\gamma_{3n}$  related to the shear strains in the cell walls via Equations (1a) and (1b), the shear stress versus strain response ( $\tau_{3n}$  versus  $\gamma_{3n}$ ) of the honeycombs follows as

$$\tau_{3n} = \left[ \sigma(\varepsilon_1^{\text{ref}}) \cos \omega + \sigma(\varepsilon_2^{\text{ref}}) \sin \omega \right] \frac{\bar{\rho}}{2\sqrt{3}}, \tag{7}$$

where  $\varepsilon_1^{\text{ref}} \equiv \gamma_{3n} \cos \omega / \sqrt{3}$  and  $\varepsilon_2^{\text{ref}} \equiv \gamma_{3n} \sin \omega / \sqrt{3}$ .

Experimental measurements by [Gerard 1948] on the shear of clamped plates suggest that employing the secant shear modulus  $G_s \equiv \tau/\gamma$  in Equation (4) gives good agreement with measured results. Thus, we estimate the plastic shear buckling stress of clamped plates as

$$\tau_c^p = \frac{k\pi^2 G_s}{6(1-\nu)} \left(\frac{t}{l}\right)^2.$$

Here,  $G_s \equiv \tau/\gamma = \sigma/3\varepsilon$  is the shear secant modulus derived from the true tensile stress versus logarithmic strain curve of the parent material and evaluated at  $\sigma = \sqrt{3}\tau_c^p$ . Assuming collapse of the square honeycomb when either the wall parallel to the  $x_1$  axis or  $x_2$  axis plastically buckles, the shear strength of the square honeycomb is

$$\tau_{3n}^p = \begin{cases} \left( \sqrt{3}\tau_c^p \cos \omega + \sigma(\varepsilon^{\text{ref}} \tan \omega) \sin \omega \right) \frac{\bar{\rho}}{2\sqrt{3}}, & \text{if } \omega \leq 45^\circ, \\ \left( \sigma(\varepsilon^{\text{ref}} \cot \omega) \cos \omega + \sqrt{3}\tau_c^p \sin \omega \right) \frac{\bar{\rho}}{2\sqrt{3}}, & 45^\circ < \omega \leq 90^\circ, \end{cases} \quad (8)$$

where  $\varepsilon^{\text{ref}}$  is the tensile strain of the solid material at a tensile stress  $\sqrt{3}\tau_c^p$ .

We emphasize that this analysis assumes uniform deformation of the cell walls of the square honeycomb and only provides an upper bound to the shear stress versus strain response. The analytical prediction for the shear stress versus strain response, Equation (7), is valid up to the onset of wrinkling and has been added to the measurements plotted in Figures 6 and 8, with the curves truncated at the plastic buckling stress (Equation (8)). The analytical model is in good agreement with the measurements but predicts the onset of wrinkling slightly before that observed in the experiments.

#### 4. Finite element predictions of the shear response

Finite element (FE) calculations of the shear response were performed using the general purpose finite element package ABAQUS Standard (Hibbitt, Karlsson & Sorensen, Inc.). All simulations reported here were performed on the unit cell shown in Figure 1b (as a cruciform section), including the nonlinear effects of large displacements. Additional calculations on larger repeating units comprising two and four unit cells gave nearly identical results to those presented here and are omitted for the sake of brevity.

The unit cell of the square honeycomb was modeled using linear 3D shell elements (S4R in the ABAQUS notation). Periodic boundary conditions were specified on the boundaries  $x_1 = \pm l/2$  and  $x_2 = \pm l/2$  by specifying that all degrees of freedom (both translational and rotational) on the edges  $x_i = -l/2$  are equal to the corresponding ones on the edge  $x_i = +l/2$ , where the subscript  $i$  ranges from 1 to 2. The nodes on the plane  $x_3 = 0$  were fully clamped. Loading was specified by prescribing the displacements  $u_1 = \delta \cos \omega$  and  $u_2 = \delta \sin \omega$ , where  $\delta$  is the applied displacement and  $\omega$  is the loading angle<sup>2</sup>, to all nodes on the plane  $x_3 = h$ . The displacements  $u_3$  of all nodes on the plane  $x_3 = h$  were constrained to be equal. The rotational degrees of the nodes on the planes  $x_3 = h$  and  $x_3 = 0$  were set to zero to simulate the constraint imposed by the honeycomb joint at the loading platens. These boundary conditions imply that the strain  $\varepsilon_{33}$  of the square honeycomb specimens is unconstrained with the average traction  $T_3 = 0$ . The single-lap shear tests discussed above provide negligible constraint to straining in the 3-direction, so the assumed boundary conditions described here are representative. Typically, the model comprised 30 shell elements in each of the  $x_1$ ,  $x_2$  and  $x_3$ -directions, giving a total of 1800 linear shell elements. Convergence studies revealed that increasing the number of elements above 1800 did not change the results appreciably.

<sup>2</sup> The applied displacements in the FE calculations are consistent with the experiments, where the shear test fixture prevents displacements in the  $x_1$  and  $x_2$  plane orthogonal to the  $\omega$  direction.

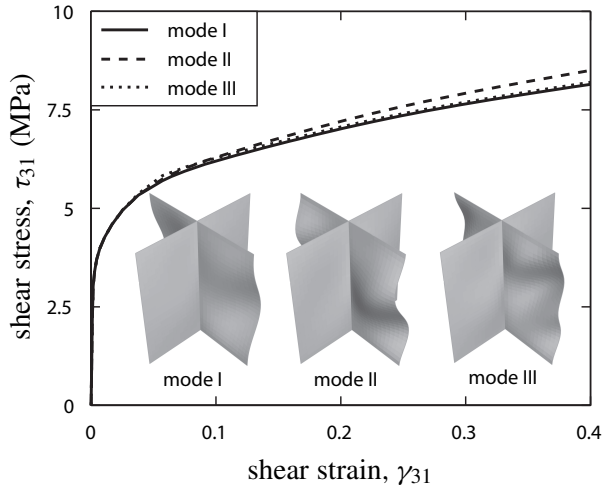


**Figure 9.** FE predictions of the shear stress  $\tau_{31}$  versus shear strain  $\gamma_{31}$  response of the  $\bar{\rho} = 0.05$  square honeycombs for three choices of the initial imperfection mode (shown in the inset). The nondimensional imperfection magnitude was taken to be  $\zeta = 0.05$  in all cases.

The uniaxial true stress versus logarithmic plastic strain was tabulated in ABAQUS using the experimentally measured response (Figure 5). J2 flow-theory was adopted. Initial imperfections were introduced into the unit cell in the form of selected elastic eigenmodes of the structure. The three imperfection modes adopted are shown in the inset of Figure 9. Mode I is the lowest frequency mode, while mode II is the next harmonic. Mode III contains the first 2 eigenmodes, with an equal maximum deflection for each mode. The maximum transverse deflection of the webs of the honeycomb for each mode is set to  $w = \zeta t$ , where  $\zeta$  is a prescribed nondimensional imperfection amplitude. The FE predictions of the  $\omega = 0^\circ$  shear stress versus strain response of the  $\bar{\rho} = 0.05$  square honeycombs are plotted in Figure 9 for the three selected modes of the initial imperfection with  $\zeta = 0.05$ . These calculations show that the response is relatively insensitive to the shape of initial imperfection. Scoping studies also revealed that the response is reasonably insensitive to the magnitude of the imperfection for  $\zeta \leq 0.1$ . In all calculations reported subsequently, we employed the mode I imperfection of Figure 9, with  $\zeta = 0.05$ .

**4.1. Comparison with measurements.** The FE predictions of the shear stress versus strain response of the square honeycombs are included in Figures 6 and 8, in which the predicted onset of wrinkling is marked by open circles. In all cases, the FE predictions agree with the experimental measurements to within about 10%. The onset of wrinkling is also accurately predicted by the FE calculations. The discrepancy between the measurements and FE predictions is greatest for the  $\bar{\rho} = 0.11$  honeycombs (Figure 6d) and is attributed to tearing of the cell walls in the experiments. This was not accounted for in the FE calculations.

A comparison between the measurements and the predictions of both the analytical model and FE calculations is summarized in Figure 10. In Figure 10a, measurements and predictions are given for the normalized shear strength  $\tau_{31}^y / (\bar{\rho} \sigma_y)$  versus  $\bar{\rho}$ , where  $\tau_{31}^y$  is the shear stress at a shear strain  $\gamma_{31} = 0.05$ ,

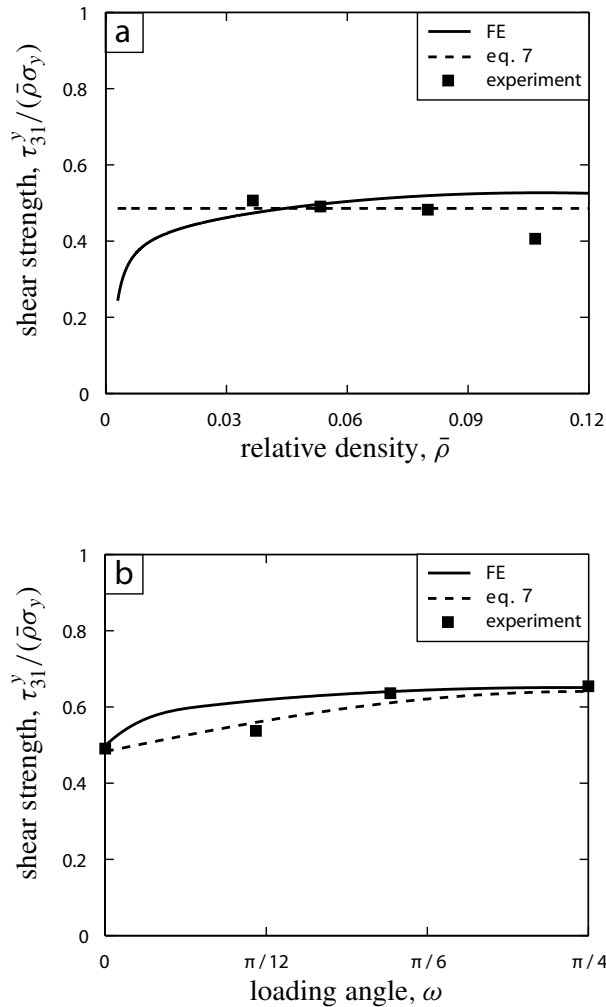


**Figure 10.** Comparison of the measured and predicted shear strengths. (a) The shear strength  $\tau_{31}^y$  at a shear strain  $\gamma_{31} = 0.05$  versus the honeycomb relative density  $\bar{\rho}$ , for  $\omega = 0$ ; (b) the shear strength  $\tau_{3n}^y$  at a shear strain  $\gamma_{3n} = 0.05$  versus the loading angle  $\omega$ , for  $\bar{\rho} = 0.05$ .

with  $\omega = 0$ . The value of 0.05 was selected for comparison purposes since the initial yield is difficult to define. Good agreement between the predictions and measurements is observed for the three lower values of  $\bar{\rho}$ , but as discussed above, tearing of the cell walls results in an over-prediction of the shear strength for the  $\bar{\rho} = 0.11$  honeycomb. The FE calculations predict a sharp drop in the shear strength for  $\bar{\rho} < 0.03$ . At these low relative densities, elastic buckling of the cell walls is expected to control the shear strength of the square honeycombs. Note that experiments at such low relative densities are impractical for usual laboratory testing: for wall thickness of, for example,  $t = 0.30$  mm, the cell size of a  $\bar{\rho} = 0.03$  honeycomb is 20 mm. Figure 10b shows a comparison between the measurements and predictions of

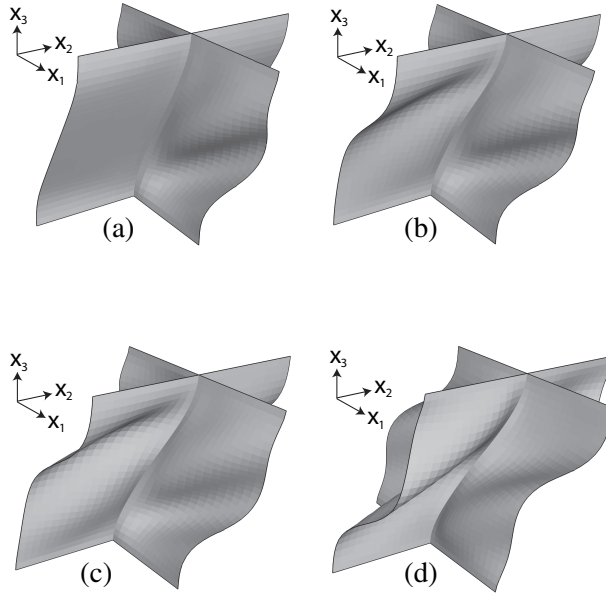


**Figure 11.** Finite element predictions of the deformation mode of the  $\bar{\rho} = 0.05$  square honeycomb at a shear strain  $\gamma_{3n} = 0.4$  for loading in the (a)  $\omega = 0^\circ$ , (b)  $\omega = \tan^{-1}(1/4)$ , (c)  $\omega = \tan^{-1}(1/2)$ , and (d)  $\omega = \pi/4$  directions.

the shear strength  $\tau_{3n}^y$  at a shear strain  $\gamma_{3n} = 0.05$  for the  $\bar{\rho} = 0.05$  square honeycombs, as a function of the loading angle  $\omega$ . We observed excellent agreement between the measurements and both the FE and analytical predictions.

Figure 11 shows the FE predictions of the deformation modes of the  $\bar{\rho} = 0.05$  square honeycomb at an applied shear strain  $\gamma_{3n} = 0.4$  for the four loading directions studied experimentally. Consistent with the experimental observations, the degree of wrinkling of the cell walls parallel to the  $x_2$  axis increases with increasing  $\omega$  as the applied load is more evenly distributed between the cell walls of the square honeycomb.

In the FE calculations we assumed that the traction  $T_3$  vanishes, with unconstrained straining of the specimen in the  $x_3$ -direction. Specimen end effects in the single-lap shear test configuration mean that this boundary condition is not satisfied over the full length of the test specimens. To assess the significance of the constraint to straining in the 3-direction imposed in the single-lap shear configuration, we compare the measurements and FE predictions of the strain  $\varepsilon_{33}$  for the  $\bar{\rho} = 0.04$  square honeycomb specimen tested in the  $\omega = 0^\circ$  direction. The strain  $\varepsilon_{33}$  from experiments was evaluated from photographs taken at selected levels of applied shear strain. Figure 12 shows a plot of  $\varepsilon_{33}$  versus the applied shear strain  $\gamma_{31}$ . Good agreement between the FE predictions and measurements suggests that the  $T_3 = 0$  boundary condition employed in the FE calculations is adequate to model our single-lap shear experiments.

**4.2. Parametric finite element study.** The FE model captures the experimental measurements within reasonable accuracy. Limitations on the specimen manufacturing and testing capabilities meant that we

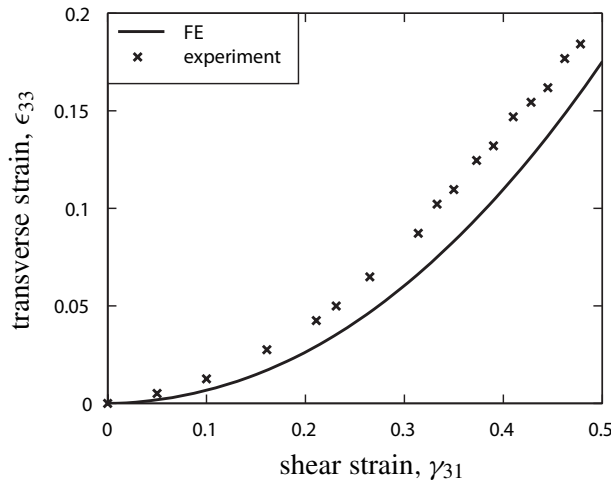


**Figure 12.** FE predictions and measurements of the through-thickness strain  $\epsilon_{33}$  versus shear strain  $\gamma_{31}$  for a  $\bar{\rho} = 0.04$  honeycomb loaded in the  $\omega = 0^\circ$  direction.

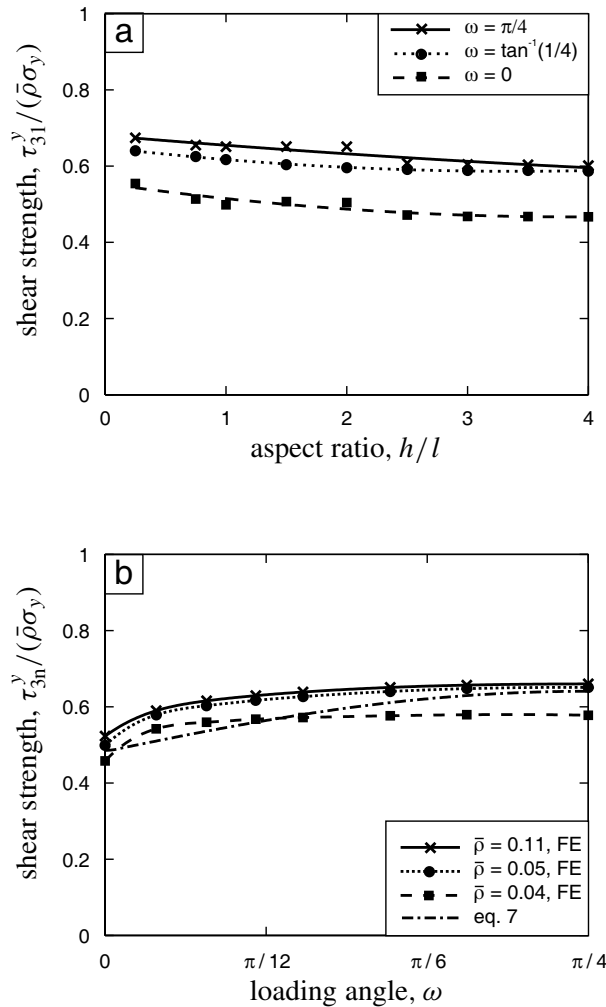
did not investigate the effect of cell aspect ratio  $h/l$  on the shear response. Also, the effect of loading direction  $\omega$  upon shear response was measured for a single value of relative density  $\bar{\rho}$ .

Figure 13a shows the FE predictions of the shear strength  $\tau_{3n}^y$  at a shear strain  $\gamma_{3n} = 0.05$  as a function of the cell aspect ratio  $h/l$  for three choices of loading angle  $\omega$ , with  $\bar{\rho}$  fixed at 0.05. The shear strength is only weakly dependent on  $h/l$ , with  $\tau_{3n}^y$  decreasing by about 10% when  $h/l$  increases from 0.25 to 4. Note that the analytical model of Equation (7) predicts no dependence of  $\tau_{3n}^y$  on  $h/l$ , which is why Figure 13a does not include these predictions. The effect of loading angle on the normalized shear strength  $\tau_{3n}^y/(\bar{\rho}\sigma_y)$  is illustrated in Figure 13b for three choices of relative density  $\bar{\rho}$ . The FE calculations and analytical predictions of Equation (7) suggest that the shear strength is reasonably insensitive to the loading direction over the range of density  $\bar{\rho}$  considered.

## 5. Comparison of the square honeycomb with competing sandwich cores

It is instructive to compare the shear strength of the stainless steel square honeycombs with competing cores. We were able to compare the measured shear strength of our stainless steel square honeycombs with data for commercially available aluminum hexagonal honeycombs, and with data for competing micro-architected sandwich cores also made from stainless steel.

The normalized shear strength  $\tau^y/(\bar{\rho}\sigma_y)$  of 5052 H39 aluminum alloy hexagonal honeycombs manufactured by Hexcel Composites is plotted against relative density  $\bar{\rho}$  in Figure 14a for loadings in two orthogonal directions. We assumed that the tensile yield strength of the parent aluminum is  $\sigma_y = 255$  MPa, as reported by [Bhat and Wang 1990]. Our experimental measurements for the shear strength of the stainless steel square honeycombs are included in Figure 14a as well. Recall that we tested four relative densities for loading in the  $\omega = 0^\circ$  direction, while the  $\bar{\rho} = 0.05$  square honeycomb was tested in the  $\omega = \pi/4$  direction. The shear strength  $\tau^y$  is defined as the peak shear strength of the aluminum honeycombs. However, the stainless steel square honeycombs display no peak shear strength, so the



**Figure 13.** FE predictions of the shear strength of the stainless steel square honeycombs. (a) Shear strength  $\tau_{31}^y$  at a shear strain  $\gamma_{31} = 0.05$  versus cell aspect ratio  $h/l$ , for selected values of the loading angle  $\omega$ , and  $\bar{\rho} = 0.05$ . (b) Shear strength  $\tau_{3n}^y$  at a shear strain  $\gamma_{3n} = 0.05$  versus loading angle  $\omega$ , for selected values of  $\bar{\rho}$ .

shear strength  $\tau^y$  is defined as the shear stress at a shear strain  $\gamma = 0.05$ . The normalized shear yield strength  $\tau^y / (\bar{\rho}\sigma_y)$  of the stainless steel honeycombs is approximately equal to the Voigt upper bound value of 0.5 (assuming the Tresca yield criterion) over the full range of relative densities investigated here. The aluminum hexagonal honeycombs are clearly weaker especially for  $\bar{\rho} < 0.06$ .

Figure 14b illustrates the effect of the core topology upon out-of-plane shear strength  $\tau^y$ . In the figure, the dependence of  $\tau^y / (\bar{\rho}\sigma_y)$  upon the relative density  $\bar{\rho}$  is given for the following cores:

- the stainless steel square honeycombs of the present study loaded in the  $\omega = 0^\circ$  direction;
- stainless steel corrugated cores [Côté et al. 2006];

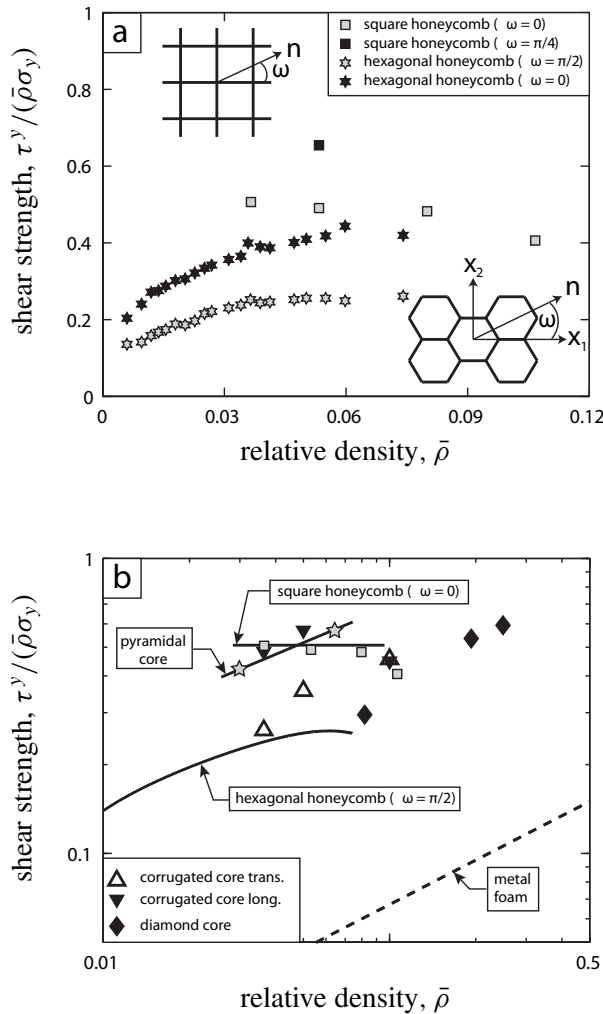


**Figure 14.** Comparison between the measured nondimensional shear strengths  $\tau^y / (\bar{\rho} \sigma_y)$  of competing sandwich cores as a function of the relative density  $\bar{\rho}$ . (a) Comparison of aluminum hexagonal honeycombs with the stainless steel square honeycombs of the present study, and (b) comparison of stainless steel micro-architected sandwich core topologies.

- AL6XN stainless steel pyramidal cores [Zok et al. 2004; Côté et al. 2007];
- aluminum hexagonal honeycomb data ( $\omega = \pi/2$ ) from Figure 14a; and
- aluminum alloy metal foams [Ashby et al. 2000].

The corrugated cores sheared in the longitudinal direction and the square honeycombs display no peak shear strength. Therefore, the shear strength  $\tau^y$  in these cases is defined as the shear stress at a shear strain  $\gamma = 0.05$ . All other cores display a peak shear strength. In these cases we define  $\tau^y$  as the peak strength.

The longitudinal shear strength of the corrugated core is comparable to that of the square honeycomb with  $\tau^y/(\bar{\rho}\sigma_y)$  and is approximately equal to the upper bound value of 0.5 (assuming the Tresca yield criterion). In transverse shear, the corrugated and diamond cores are weaker than the square honeycomb.

## 6. Concluding remarks

We manufactured square honeycombs with a cell aspect ratio  $h/l = 1$  by slotting together sheets of 304 stainless steel and then brazing the assembly. We then tested four relative densities of these honeycombs in out-of-plane shear in four loading directions. The measurements reveal that shear strength of the square honeycombs scales approximately linearly with the relative density  $\bar{\rho}$  of the honeycomb. Moreover, the shear strength of these honeycombs is nearly isotropic.

A simple analytical model based upon uniform deformation of the cell walls is in good agreement with the measurements prior to wrinkling of the cell walls. A plastic buckling analysis predicts the onset of wrinkling with reasonable accuracy. FE calculations of the shear response of the square honeycombs agree with the test measurements, and show that the shear strength of the square honeycombs is relatively insensitive to the cell aspect ratio for aspect ratios in the range  $0.5 \leq h/l \leq 4$ .

The square honeycomb design exploits the strain hardening behavior of the parent material extremely efficiently in both out-of-plane compression [Côté et al. 2004] and in out-of-plane shear. In fact, the shear strength of these honeycombs is equal to that of the corrugated core sheared in the longitudinal direction. Unlike the corrugated core, which has a low transverse shear strength [Côté et al. 2006], the shear strength of the square honeycombs is nearly isotropic. Thus, square honeycombs have great potential for application in sandwich construction.

## References

- [Ashby et al. 2000] M. Ashby, A. G. Evans, N. A. Fleck, L. J. Gibson, J. W. Hutchinson, and H. N. G. Wadley, *Metal foams: A design guide*, Butterworth Heinemann, Oxford, 2000.
- [ASTM 2000] “Standard test method for shear properties of sandwich core materials”, standard C273-00, American Society for Testing and Materials, 2000.
- [Bhat and Wang 1990] B. T. Bhat and T. G. Wang, “A comparison of mechanical properties of some foams and honeycombs”, *J. Mater. Sci.* **25**:12 (1990), 5157–5162.
- [Côté et al. 2004] F. Côté, V. S. Deshpande, N. A. Fleck, and A. G. Evans, “The out-of-plane compressive behavior of metallic honeycombs”, *Mater. Sci. Eng. A* **380**:1–2 (2004), 272–280.
- [Côté et al. 2006] F. Côté, V. S. Deshpande, N. A. Fleck, and A. G. Evans, “The compressive and shear responses of corrugated and diamond lattice materials”, *Int. J. Solids Struct.* **43**:20 (2006), 6220–6242.
- [Côté et al. 2007] F. Côté, N. A. Fleck, and V. S. Deshpande, “Fatigue performance of sandwich beams with a pyramidal core”, *Int. J. Fatigue* (2007). In press.
- [Doyoyo and Mohr 2003] M. Doyoyo and D. Mohr, “Microstructural response of aluminum honeycomb to combined out-of-plane loading”, *Mech. Mater.* **35**:9 (2003), 865–876.
- [Evans et al. 2001] A. G. Evans, J. W. Hutchinson, N. A. Fleck, M. F. Ashby, and H. N. G. Wadley, “The topological design of multifunctional cellular metals”, *Prog. Mater. Sci.* **46**:3–4 (2001), 309–327.
- [Fleck and Deshpande 2004] N. A. Fleck and V. S. Deshpande, “The resistance of clamped sandwich beams to shock loading”, *J. Appl. Mech. (ASME)* **71**:3 (2004), 386–401.
- [Gerard 1948] G. Gerard, “Critical shear stress of plates above the proportional limit”, *J. Appl. Mech. (ASME)* **15** (1948), 7–12.

- [Gibson and Ashby 1997] L. J. Gibson and M. F. Ashby, *Cellular solids, structure and properties*, 2nd ed., Cambridge University Press, Cambridge, 1997.
- [Hexcel 1999] “HexWeb honeycomb attributes and properties”, publication TSB-120, Hexcel Composites, Pleasanton, CA, 1999.
- [Kelsey et al. 1958] S. Kelsey, R. A. Gellatly, and B. W. Clark, “The shear modulus of foil honeycomb cores”, *Aircraft Eng.* **30** (1958), 294–302.
- [Mohr and Doyoyo 2004a] D. Mohr and M. Doyoyo, “Deformation-induced folding systems in thin-walled monolithic hexagonal metallic honeycomb”, *Int. J. Solids Struct.* **41**:11–12 (2004), 3353–3377.
- [Mohr and Doyoyo 2004b] D. Mohr and M. Doyoyo, “Experimental investigation on the plasticity of hexagonal aluminum honeycomb under multiaxial loading”, *J. Appl. Mech. (ASME)* **71**:3 (2004), 375–385.
- [Timoshenko and Gere 1963] S. P. Timoshenko and J. M. Gere, *Theory of elastic stability*, 2nd ed., McGraw Hill, New York, 1963.
- [Werren and Norris 1950] F. Werren and C. B. Norris, “Analysis of shear strength of honeycomb cores for sandwich constructions”, Technical Report 2208, NACA, 1950, Available at <http://hdl.handle.net/2060/19930082855>.
- [Xue and Hutchinson 2004] Z. Xue and J. W. Hutchinson, “A comparative study of impulse-resistant metal sandwich plates”, *Int. J. Impact Eng.* **30**:10 (2004), 1283–1305.
- [Zhang and Ashby 1992] J. Zhang and M. F. Ashby, “The out-of-plane properties of honeycombs”, *Int. J. Mech. Sci.* **34**:6 (1992), 475–489.
- [Zhuang and Eagar 1997] W. D. Zhuang and T. W. Eagar, “Transient liquid-phase bonding using coated metal powders”, *Weld. J.* **76**:4 (1997), 157s–162s.
- [Zok et al. 2004] F. W. Zok, S. A. Waltner, Z. Wei, H. J. Rathbun, R. M. McMeeking, and A. G. Evans, “A protocol for characterizing the structural performance of metallic sandwich panels: Application to pyramidal truss cores”, *Int. J. Solids Struct.* **41**:22–23 (2004), 6249–6271.

Received 17 Feb 2006. Accepted 12 May 2006.

FRANÇOIS COTE: [fc248@eng.cam.ac.uk](mailto:fc248@eng.cam.ac.uk)

Cambridge University Engineering Department, Trumpington Street, Cambridge, CB2 1PZ, United Kingdom

VIKRAM S. DESHPANDE: [vsd@eng.cam.ac.uk](mailto:vsd@eng.cam.ac.uk)

Cambridge University Engineering Department, Trumpington Street, Cambridge, CB2 1PZ, United Kingdom

NORMAN A. FLECK: [naf1@eng.cam.ac.uk](mailto:naf1@eng.cam.ac.uk)

Cambridge University Engineering Department, Trumpington Street, Cambridge, CB2 1PZ, United Kingdom